TECHNISCHE MECHANIK, Band 23, Heft 2-4, (2003), 103-112
Manuskripteingang: 23. Juni 2003

Continuum Thermodynamic Modeling and Simulation of Electromagnetic Metal Forming

Dedicated to the memory of our friend and mentor Jürgen Olschewski

B. Svendsen, T. Chanda

The purpose of this work is the formulation and application of a continuum field approach to the phenomenological modeling of a class of engineering materials which can be dynamically formed using strong magnetic fields. This is done in the framework of a thermodynamic, internal-variable-based formulation in which the deformation, temperature and magnetic fields are in general coupled. As is well-known, this coupling takes the form of the Lorentz force as an additional supply of momentum, and the electromotive power as an additional supply of energy, in the material. The constitutive formulation is based as usual on the exploitation of the dissipation principle, here for the case of generally anisotropic, elastoviscoplastic material behaviour. In particular, the general results so obtained are applied in particular to the case of small strain and large rotation. As shown here, in this special case, the electromagnetic field relations become independent of the deformation field. As such, they can be solved independently and used as input for the solution of the thermomechanical field relations. Application of this reduced formulation for small strain to the simulation of the electromagnetic forming of an aluminum tube shows the importance of accounting for inertial effects and rate-dependence in the modeling.

1 Introduction

Electromagnetic forming (EMF) is a dynamic, high-strain-rate forming method in which strain-rates of $\geq 10^3$ s^{-1} are achieved. In this process, deformation of the workpiece is driven by the interaction of a current generated in the workpiece with a magnetic field generated by a coil adjacent to the workpiece. In particular, the interaction of these two fields results in a material body force, *i.e.*, the Lorenz force, representing an additional supply of momentum to the material resulting in deformation. EMF is but one of a number of high deformation-rate forming methods which offer certain advantages over other forming methods such as increase in formability for certain kinds of materials, reduction in wrinkling, the ability to combine forming and assembly operations, and many others.

Modeling and simulation work in this area has focused primarily on the structural and coupled-field aspects of the problem (*e.g.*, Gourdin, 1989; Gourdin *et al.*, 1989; Takata *et al.*, 1988; Fenton & Daehn, 1998) has focused mainly on the structural and coupled-field aspects of the problem. The material modeling, in constrast, is generally one-dimensional and identified with the help of uniaxial tension-compression tests. Fenton & Daehn (1998), for example, utilize the Steinberg model, which is a one-dimensional, purely mechanical stress-strain independent of the strain rate. It is just such rate-dependence, however, which is characteristic of the behaviour of metallic materials at high forming rates such as those achieved during EMF. As such, from a phenomenological point of view, the relevant material behaviour here is elastoviscoplasticity. The main purpose of the current work is to outline a continuum thermomechanical framework and formulation for the modeling of dynamic deformation induced by strong magnetic fields and apply this to the simulation of the electromagnetic forming of an aluminium tube. In particular, emphasis is placed here on the modeling aspects; details on the algorithmic formulation and numerical implementation will be presented elsewhere (Brosius *et al.*, 2003).

2 Basic Field Formulation and Results

Of principle interest in this work is the continuum modeling of the dynamic interaction of strong external electromagnetic fields with metallic solids resulting in their deformation. To this end, the system consisting of ambient space and solid components is modeled as an electromagnetic composite. Further, each of the solid components is modeled as a continuum with additional degrees of freedom represented by the electromagnetic fields. In this case, the usual thermomechanical balance relations to be formulated in what follows are extended by Maxwell's electromagnetic field relations. In general, solution of these relations yields wave-like electromagnetic fields. For all

problems of interest here, however, the frequencies of relevance (*i.e.*, less than 10 MHz) correspond to electromagnetic wavelengths which are much larger than the relevant structures. As such, the wave character is insignificant, and can be neglected here. This represents the so-called quasistatic approximation (Moon, 1980, §2.2 and §8.2) in the current context. In this case, the formulation then becomes independent of the dielectric displacement. In addition, for the class of electric conductors of interest here, (*e.g.*, aluminum, copper), any charge decays away so quickly in comparison to any other process that it can be reasonably be neglected from the start. Furthermore, these materials are non-polarizing and non-magnetizing. Lastly, the processes of interest here (*e.g.*, electromagnetic metal forming) are all non-relativistic. On the basis of these assumptions, then, we have the reduced system

$$\begin{aligned} \mathbf{0} &= \dot{\boldsymbol{b}} + \operatorname{curl} \boldsymbol{e} \,, \\ 0 &= \operatorname{div} \boldsymbol{b} \,, \\ \boldsymbol{j} &= \operatorname{curl} \boldsymbol{h} \,, \\ 0 &= \operatorname{div} \boldsymbol{j} \,, \end{aligned} \tag{2.1}$$

of Maxwell's relations in any materially homogeneous region of the composite (*e.g.*, Hutter & van de Ven, 1978, Ch. 1; Müller, 1985, Ch. 9; Eringen & Maugin, 1990, Ch. 3). These represent, respectively, surface conservation of magnetic flux (Faraday's law), volume conservation of magnetic flux (no free magnetic poles), surface conservation of electrical charge (Maxwell's generalization of Ampere's law), and volume conservation of electrical charge, respectively, again for the case of no free charge, polarization or magnetization. In these relations, $\boldsymbol{e}$ represents the electromotive intensity, $\boldsymbol{h}$ the magnetic field strength, $\boldsymbol{b}$ the magnetic induction or flux density, and

$$\boldsymbol{j} = \boldsymbol{j}_{\text{K}} + \boldsymbol{j}_{\text{A}} \tag{2.2}$$

the conductive current. As indicated, this latter quantity generally splits into constitutive $\boldsymbol{j}_{\text{K}}$ and applied $\boldsymbol{j}_{\text{A}}$ parts. Lastly, treating the material under consideration as electromagnetically isotropic, the corresponding isotropic (constitutive) Maxwell-Lorentz relation

$$\boldsymbol{b} = J\, \mu_{\text{EM}}\, \boldsymbol{C}^{-1} \boldsymbol{h} \tag{2.3}$$

relative to an inertial (Lorentz) frame, again in the non-relativistic limit, applies. Here, $\boldsymbol{C} := \boldsymbol{F}^{\text{T}} \boldsymbol{F}$ represents the right Cauchy-Green deformation, $\boldsymbol{F}$ the deformation gradient, $J := \det(\boldsymbol{F})$, and μ_{EM} is the magnetic permeability.

Consider next the formulation of continuum balance relations. For simplicity, attention is restricted here to isothermal conditions. For the case at hand, interaction between electromagnetic and mechanical fields takes the forms of the Lorenz force and electromotive power. Indeed, the effective force represented by $\boldsymbol{b}$ acting on current in the material results in an additional body force (density) $\boldsymbol{F}^{-\text{T}}(\boldsymbol{j} \times \boldsymbol{b})$ on the material (*i.e.*, the Lorentz force density), where $\boldsymbol{F}$ represents the deformation gradient. Analogously, the effective force represented by $\boldsymbol{e}$ acting on the current in the material results in an additional power expenditure with density $\boldsymbol{j} \cdot \boldsymbol{e}$ (*i.e.*, the electromotive power). On this basis, in any materially-homogeneous region of the composite not containing a singular surface, the local forms

$$\begin{aligned} \dot{\varrho} &= 0 \,, \\ \varrho\, \ddot{\boldsymbol{\xi}} &= \boldsymbol{F}^{-\text{T}}(\boldsymbol{j} \times \boldsymbol{b}) + \operatorname{div}(\boldsymbol{F}\boldsymbol{S}) = \operatorname{div}(\boldsymbol{F}\boldsymbol{S} + \boldsymbol{M}) \,, \end{aligned} \tag{2.4}$$

for mass and momentum balance, respectively, hold, together with the symmetry of $\boldsymbol{S}$. Here, $\boldsymbol{\xi}$ represents the motion/deformation field, $\dot{\boldsymbol{\xi}}$ the material velocity, and $\boldsymbol{S}$ the second Piola-Kirchhoff stress. Further, we have the Lorentz force $\boldsymbol{F}^{-\text{T}}(\boldsymbol{j} \times \boldsymbol{b})$, and the Maxwell stress

$$\boldsymbol{M} := \boldsymbol{F}^{-\text{T}} \boldsymbol{h} \otimes \boldsymbol{b} - \tfrac{1}{2}\, (\boldsymbol{h} \cdot \boldsymbol{b}) \boldsymbol{F}^{-\text{T}} \,. \tag{2.5}$$

Using rationalized MKSA units (*e.g.*, Jackson, 1975, Appendix), note that $\boldsymbol{b}$ has units of volt s m^{-2}, and $\boldsymbol{h}$ units of coul m^{-1} s^{-1} = amp m^{-1} with amp = coul s^{-1}. Since volt = N m coul^{-1}, $\boldsymbol{M}$ has units of coul volt m^{-3} = N m^{-2}, and μ_{EM} has units of volt s amp^{-1} m^{-1} = N amp^{-2}. In free space, for example, $\mu_{\text{EM}} = 4\pi \times 10^{-7}$ N amp^{-2}.

3 Basic Constitutive Formulation and Results

The formulation to follow pertains to anisotropic viscoelastoplastic material behaviour of electrically-conducting materials (*e.g.*, aluminum) without free charge, polarization or magnetization. For this case, we have the basic

material frame-indifferent form

$$\mathcal{C} = \mathcal{C}(\boldsymbol{C}, \boldsymbol{\alpha}, \dot{\boldsymbol{C}}, \dot{\boldsymbol{\alpha}}, \boldsymbol{b}, \boldsymbol{e}) \tag{3.1}$$

for the dependent constitutive quantities $\boldsymbol{S}$ and ψ. Here, $\boldsymbol{\alpha}$ represents a set of deformation-like internal variables accounting in an effective fashion for the effects of inelastic processes such as isotropic and kinematic hardening, or damage, on the macroscopic material behaviour. In the present isothermal anisotropic context, restrictions on the form of (3.1) are obtained here with the help of the Clausius-Duhem form

$$\delta = \tfrac{1}{2}\, \boldsymbol{S} \cdot \dot{\boldsymbol{C}} + \boldsymbol{j} \cdot \boldsymbol{e} - \dot{\psi} \tag{3.2}$$

for the dissipation rate density δ in the current context. Here, $\boldsymbol{j} \cdot \boldsymbol{e}$ represents the electromotive power, and ψ the referential free energy density. In the context of (3.1) and (3.2), application of the Coleman-Noll dissipation principle to the current case (see Svendsen & Chanda, 2003, for details) leads to the reduced form

$$\psi = \psi(\theta, \boldsymbol{C}, \boldsymbol{\alpha}) \tag{3.3}$$

for ψ, as well as that

$$\delta = \tfrac{1}{2}\, (\boldsymbol{S} - 2\, \psi_{,\boldsymbol{C}}) \cdot \dot{\boldsymbol{C}} + \boldsymbol{\varsigma} \cdot \dot{\boldsymbol{\alpha}} + \boldsymbol{j} \cdot \boldsymbol{e} \tag{3.4}$$

for δ, with

$$\boldsymbol{\varsigma} := -\psi_{,\boldsymbol{\alpha}} \tag{3.5}$$

the thermodynamic conjugate to $\boldsymbol{\alpha}$. On the basis of (3.1) and (3.4), the constitutive model is completed by the dissipation potential

$$d = d(\boldsymbol{C}, \boldsymbol{\alpha}, \dot{\boldsymbol{C}}, \dot{\boldsymbol{\alpha}}, \boldsymbol{b}, \boldsymbol{e}) \tag{3.6}$$

(*e.g.*, Edelen, 1973; Šilhavý, 1997, §12.3). Together with ψ from (3.3), d determines the constitutive forms[1]

$$\begin{aligned} \boldsymbol{S} &= 2\, \varphi_{,\dot{\boldsymbol{C}}}\,, \\ \boldsymbol{0} &= \varphi_{,\dot{\boldsymbol{\alpha}}}\,, \\ \boldsymbol{j}_{\mathrm{K}} &= \varphi_{,\boldsymbol{e}}\,, \end{aligned} \tag{3.7}$$

via the rate potential

$$\varphi := \dot{\psi} + d\,. \tag{3.8}$$

In turn, these yield the constitutive form

$$\delta = d_{,\dot{\boldsymbol{C}}} \cdot \dot{\boldsymbol{C}} + d_{,\dot{\boldsymbol{\alpha}}} \cdot \dot{\boldsymbol{\alpha}} + d_{,\boldsymbol{e}} \cdot \boldsymbol{e} + \boldsymbol{j}_{\mathrm{A}} \cdot \boldsymbol{e} \tag{3.9}$$

for the dissipation rate density from (3.4). For simplicity, attention is restricted in this work to the class of materials whose dynamic behaviour can be described by the additive split

$$d(\boldsymbol{C}, \boldsymbol{\alpha}, \dot{\boldsymbol{C}}, \dot{\boldsymbol{\alpha}}, \boldsymbol{b}, \boldsymbol{e}) = d_{\mathrm{Int}}(\boldsymbol{C}, \boldsymbol{\alpha}, \dot{\boldsymbol{C}}, \dot{\boldsymbol{\alpha}}) + d_{\mathrm{EM}}(\boldsymbol{C}, \boldsymbol{\alpha}, \boldsymbol{b}, \boldsymbol{e}) \tag{3.10}$$

of d into internal d_{Int} and electromagnetic d_{EM} parts. For example, this is the case when we work with Ohm's law for the constitutive part of $\boldsymbol{j}$, *i.e.*,

$$\boldsymbol{j}_{\mathrm{K}} = J\, \sigma_{\mathrm{EM}}(\theta, \boldsymbol{C}, \boldsymbol{\alpha})\, \boldsymbol{C}^{-1} \boldsymbol{e} \tag{3.11}$$

where σ_{EM} is the electrical conductivity of the material. In these, any thermoelectric or magnetostriction effects are neglected. This is reasonable for conductors such as aluminum or copper at room temperature and "low" magnetic fields. Since $\boldsymbol{j}$ has units of amp m^{-2}, note that σ_{EM} has units of amp volt^{-1} m^{-1} $= \Omega^{-1}$ m^{-1} with $\Omega = 1$ Ohm $=$ volt amp^{-1}. Again, for most metals $\sigma_{\mathrm{EM}} \approx 10^7$.

Among the constitutive forms (3.7), note that $(3.7)_2$ represents an implicit or "weak" constitutive relation for $\dot{\boldsymbol{\alpha}}$ via (3.3). In particular, since $\varphi_{,\dot{\boldsymbol{\alpha}}\dot{\boldsymbol{\alpha}}} = d_{\mathrm{Int},\dot{\boldsymbol{\alpha}}\dot{\boldsymbol{\alpha}}}$ is (at least) positive semi-definite via the convexity of d in this argument, $\dot{\boldsymbol{\alpha}}$ minimizes φ. In any case, the constitutive relation for $\boldsymbol{\alpha}$ involved can also be expressed in the explicit form

$$\dot{\boldsymbol{\alpha}} = \phi_{,\boldsymbol{\varsigma}} \tag{3.12}$$

[1] In general, d will not be globally differentiable in its non-equilibrium arguments. In this case, the potential relations (3.7) will take the weaker, more general form of subdifferentials. For simplicity, however, we use the partial derivative notation and point out the exceptions explicitly in what follows.

in terms of the potential

$$\phi(\boldsymbol{C},\boldsymbol{\alpha},\dot{\boldsymbol{C}},\boldsymbol{\varsigma}) = \boldsymbol{\varsigma}\cdot\dot{\boldsymbol{\alpha}} - d_{\text{Int}}(\boldsymbol{C},\boldsymbol{\alpha},\dot{\boldsymbol{C}},\dot{\boldsymbol{\alpha}}) \tag{3.13}$$

Legendre (thermodynamic) conjugate to d_{Int}. From a thermodynamic point of view, (3.12) implies that $\boldsymbol{\varsigma}$ represents the driving force for the evolution of $\boldsymbol{\alpha}$.

4 Special Case: Elastoviscoplasticity at Small Strain

To investigate the consequences of the general results from the last two sections in a concrete setting, these are specialized now to the case of small strain and (possibly) large rotation. Indeed, certain kinds of applications such as the electromagnetic forming of a metal tube to be discussed below in §5 can be well-approximated by such an assumption. In this case, we have $\boldsymbol{F} \approx \boldsymbol{R}$, $J \approx 1$ and $\boldsymbol{C} \approx \boldsymbol{I} + 2\,\boldsymbol{E}$ with $\boldsymbol{E} := \text{sym}(\boldsymbol{F} - \boldsymbol{I})$ as usual. In turn,

$$\boldsymbol{S} \approx \varphi_{,\dot{\boldsymbol{E}}} \tag{4.1}$$

then follows for the second Piola-Kirchhoff stress via $(3.7)_1$. In addition, the simplified constitutive forms

$$\begin{aligned} \boldsymbol{b} &= \mu_{\text{EM}}\,\boldsymbol{h}\,, \\ \boldsymbol{j}_{\text{K}} &= \sigma_{\text{EM}}\,\boldsymbol{e}\,, \end{aligned} \tag{4.2}$$

for $\boldsymbol{b}$ and $\boldsymbol{j}_{\text{K}}$, respectively, then follow from $(2.3)_2$ and (3.11), respectively. As such, the referential Maxwell-Lorentz relations are independent of the deformation field in this case.

Consider next the local field relations $(2.4)_2$ for the motion/deformation field $\boldsymbol{\xi}$, and (2.1) for the electromagnetic fields, in the current context of small strain. As usual, the satisfaction of $(2.1)_2$ is obtained identically when we work with the potential relation

$$\boldsymbol{b} = \text{curl}\,\boldsymbol{a} \tag{4.3}$$

(*e.g.*, Jackson, 1975, §6.4) for the magnetic flux $\boldsymbol{b}$. In addition, $(2.1)_1$ is then satisfied identically by the potential form

$$\boldsymbol{e} = -\dot{\boldsymbol{a}} - \nabla\dot{\chi} \tag{4.4}$$

for $\boldsymbol{e}$ in terms of $\boldsymbol{a}$ and the scalar potential χ. Combining $(2.1)_3$, $(4.2)_{1,2}$, (4.3), and (4.4) results in the inhomogeneous "diffusion" equation

$$\sigma_{\text{EM}}\,\dot{\boldsymbol{a}} + \text{curl}(\mu_{\text{EM}}^{-1}\,\text{curl}\,\boldsymbol{a}) = \boldsymbol{j}_{\text{A}} - \sigma_{\text{EM}}\,\nabla\dot{\chi} \tag{4.5}$$

via (2.2) for $\boldsymbol{a}$ which is independent of the deformation gradient $\boldsymbol{F}$. The weak form of this is with respect to a materially-homogeneous region B is given by

$$\int_B \{\sigma_{\text{EM}}\,\dot{\boldsymbol{a}} - (\boldsymbol{j}_{\text{A}} - \sigma_{\text{EM}}\,\nabla\dot{\chi})\}\cdot\boldsymbol{a}_* + \int_B \mu_{\text{EM}}^{-1}\,\text{curl}\,\boldsymbol{a}\cdot\text{curl}\,\boldsymbol{a}_* = 0 \tag{4.6}$$

via $(4.2)_1$ and (4.3) for all test fields $\boldsymbol{a}_*$ assuming the natural boundary conditions $\boldsymbol{h}_{\partial B_{\text{c}}}\times\boldsymbol{n}_{\partial B_{\text{c}}} = \boldsymbol{0}$ at the current boundary ∂B_{c}. Except for the boundary condition, note that the weak form (4.6) for $\boldsymbol{a}$ is independent of $\boldsymbol{\xi}$. Besides $\boldsymbol{j}_{\text{A}}$, $\nabla\dot{\chi}$ is considered known, *e.g.*, via a gauge condition. As already mentioned, (4.5) and so (4.6) are parabolic or diffusive in nature, with $1/\mu_{\text{EM}}\,\sigma_{\text{EM}}$ representing the "magnetic" diffusivity. In this case, the initial vector potential and so magnetic field will decay away on a timescale given by $\ell^2\mu_{\text{EM}}\,\sigma_{\text{EM}}$, where ℓ is a characteristic lengthscale for the spatial variation of $\boldsymbol{h}$.

The weak form (4.6) for $\boldsymbol{a}$ is completed here by those

$$\int_B \{\varrho\,\ddot{\boldsymbol{\xi}} - \boldsymbol{R}(\boldsymbol{j}\times\boldsymbol{b})\}\cdot\boldsymbol{\xi}_* + \int_B \boldsymbol{R}\boldsymbol{S}\cdot\nabla\boldsymbol{\xi}_* = 0 \tag{4.7}$$

of momentum balance $(2.4)_1$ with respect to the corresponding test field $\boldsymbol{\xi}_*$ assuming traction-free boundaries. From (4.3) and (4.4), one obtains the expression

$$\boldsymbol{R}(\boldsymbol{j}\times\boldsymbol{b}) = \boldsymbol{R}[(\boldsymbol{j}_{\text{A}} - \sigma_{\text{EM}}\,\nabla\dot{\chi} - \sigma_{\text{EM}}\,\dot{\boldsymbol{a}})\times\text{curl}\,\boldsymbol{a}] \tag{4.8}$$

for the Lorentz force in terms of $\boldsymbol{a}$, $\dot{\chi}$ and $\boldsymbol{j}_{\text{A}}$. Alternatively, $(4.7)_1$ takes the form

$$\int_B \varrho\,\ddot{\boldsymbol{\xi}}\cdot\boldsymbol{\xi}_* + \int_B \boldsymbol{R}\boldsymbol{S}\cdot\nabla\boldsymbol{\xi}_* = \int_{\partial B}\{(\boldsymbol{b}_{\partial B_{\text{c}}}\cdot\boldsymbol{n}_{\partial B_{\text{c}}})\,\boldsymbol{h}_{\partial B_{\text{c}}} - p_{\partial B_{\text{c}}}\boldsymbol{n}_{\partial B_{\text{c}}}\}\cdot\boldsymbol{\xi}_* \tag{4.9}$$

following from $(2.4)_2$, where

$$p_{\partial B_{\mathrm{c}}} := \tfrac{1}{2}\,(\boldsymbol{b}_{\partial B_{\mathrm{c}}} \cdot \boldsymbol{h}_{\partial B_{\mathrm{c}}}) = \tfrac{1}{2}\,\mu_{\mathrm{EM}}\,\boldsymbol{h}_{\partial B_{\mathrm{c}}} \cdot \boldsymbol{h}_{\partial B_{\mathrm{c}}} \tag{4.10}$$

represents the so-called magnetic pressure. The form (4.9) implies that, if $\boldsymbol{b}_{\partial B_{\mathrm{c}}}$ is parallel to ∂B_{c}, such that $\boldsymbol{b}_{\partial B_{\mathrm{c}}} \cdot \boldsymbol{n}_{\partial B_{\mathrm{c}}} = 0$, then the Lorenz force is equivalent to a pressure at the boundary. This is exactly the type of boundary condition realized in certain types of applications, *e.g.*, certain types of electromagnetic metal forming (*e.g.*, Fenton & Daehn, 1998; Beerwald *et al.*, 2000). In general, however, this will not be the case.

Next, we turn to the concrete forms of the free energy density ψ from (3.3) and inelastic potential ϕ from (3.13), again for the special case of thermoelastoviscoplasticity with isotropic hardening here. A number of models, both micromechanical (*e.g.*, Bruhns & Diehl, 1989) and phenomenological (*e.g.*, Lemaitre & Chaboche, 1990) in nature, for such material behaviour can be found in the literature. In the current context, this case is represented by the choice $\boldsymbol{\alpha} = (\epsilon_{\mathrm{P}}, \boldsymbol{E}_{\mathrm{P}})$, with ϵ_{P} the local equivalent accumulated inelastic strain as a measure of isotropic hardening, and $\boldsymbol{E}_{\mathrm{P}}$ the local inelastic strain. On this basis, we work with the corresponding form

$$\psi = \psi(\boldsymbol{E}, \epsilon_{\mathrm{P}}, \boldsymbol{E}_{\mathrm{P}}) \tag{4.11}$$

for the free energy density, again from (3.3) reduced to the current context of small strain. Now, in the context of small strain, the difference

$$\boldsymbol{E}_{\mathrm{E}} := \boldsymbol{E} - \boldsymbol{E}_{\mathrm{P}} \tag{4.12}$$

is associated with the elastic strain in the material. As such, the energy stored in the material during loading is dependent on $\boldsymbol{E}_{\mathrm{E}}$. In this case, the free energy ψ as given in (4.11) reduces to a function of $\boldsymbol{E}_{\mathrm{E}}$ alone, *i.e.*,

$$\psi(\boldsymbol{E}, \epsilon_{\mathrm{P}}, \boldsymbol{E}_{\mathrm{P}}) = \psi_{\mathrm{I}}(\boldsymbol{E}_{\mathrm{E}}, \epsilon_{\mathrm{P}})\ . \tag{4.13}$$

From a different point of view, $\boldsymbol{E}_{\mathrm{P}}$ represents in this case a so-called elastic material isomorphism (*e.g.*, Wang & Bloom, 1974; Bertram, 1993; Svendsen, 1998), implying that the form of the elastic material response is unaffected by $\boldsymbol{E}_{\mathrm{P}}$. Assuming further that inelastic processes contributing to the evolution of ϵ_{P}, and so to isotropic hardening, do not affect the elastic response of the material, we have the split

$$\psi_{\mathrm{I}}(\boldsymbol{E}_{\mathrm{E}}, \epsilon_{\mathrm{P}}) = \psi_{\mathrm{E}}(\boldsymbol{E}_{\mathrm{E}}) + \psi_{\mathrm{P}}(\epsilon_{\mathrm{P}}) \tag{4.14}$$

of ψ_{I} into elastic ψ_{E} and inelastic ψ_{P} parts, with

$$\psi_{\mathrm{E}}(\boldsymbol{E}_{\mathrm{E}}) = \tfrac{1}{2}\,\lambda\,(\boldsymbol{I} \cdot \boldsymbol{E}_{\mathrm{E}})^2 + \mu\,\boldsymbol{E}_{\mathrm{E}} \cdot \boldsymbol{E}_{\mathrm{E}} \tag{4.15}$$

the usual Hooke form of ψ_{E}. Here, λ and μ represents Lame's constants. In turn, (4.14) determines the forms

$$\begin{aligned} \boldsymbol{T}_{\mathrm{P}} &:= -\psi_{,\boldsymbol{E}_{\mathrm{P}}}\ , \\ \varsigma_{\mathrm{P}} &:= -\psi_{,\epsilon_{\mathrm{P}}}\ , \end{aligned} \tag{4.16}$$

for the stress-like internal variables via (3.5) reduced to the current context. In particular, $-\varsigma_{\mathrm{P}}$ represents the flow stress.

Consider next the form of the inelastic potential ϕ from (3.13). Restricting attention to the case of rate-dependent metallic materials here, the transition to inelastic behaviour can be modeled as an activation process. One common phenomenological form for such a potential in this case is a power-law relation, *e.g.*,

$$\phi(\epsilon_{\mathrm{P}}, \dot{\boldsymbol{E}}, \boldsymbol{T}_{\mathrm{P}}, \varsigma_{\mathrm{P}}) = \frac{\gamma(\epsilon_{\mathrm{P}}, \dot{\boldsymbol{E}})\,\tau(\epsilon_{\mathrm{P}}, \dot{\boldsymbol{E}})}{m(\epsilon_{\mathrm{P}}, \dot{\boldsymbol{E}}) + 1} \langle f(\epsilon_{\mathrm{P}}, \dot{\boldsymbol{E}}, \boldsymbol{T}_{\mathrm{P}}, \varsigma_{\mathrm{P}})\rangle^{m(\epsilon_{\mathrm{P}}, \dot{\boldsymbol{E}})+1}\ , \tag{4.17}$$

with

$$f(\epsilon_{\mathrm{P}}, \dot{\boldsymbol{E}}, \boldsymbol{T}_{\mathrm{P}}, \varsigma_{\mathrm{P}}) := \sqrt{\tfrac{2}{3}}\,\frac{\sigma_{\mathrm{vM}}(\boldsymbol{T}_{\mathrm{P}}) + \varsigma_{\mathrm{P}}}{\tau(\epsilon_{\mathrm{P}}, \dot{\boldsymbol{E}})} \tag{4.18}$$

the activation function. In (4.17), γ represents a characteristic strain-rate, $\langle x\rangle := \frac{1}{2}\,(x + |x|)$ the MaCauley bracket, m the strain-rate exponent, τ the characteristic or effective activation stress or energy density scale, and

$$\sigma_{\mathrm{vM}}(\boldsymbol{T}_{\mathrm{P}}) := \sqrt{-3\,I\!I_{\mathrm{dev}(\boldsymbol{T}_{\mathrm{P}})}} = \sqrt{\tfrac{3}{2}\,I_{\mathrm{dev}(\boldsymbol{T}_{\mathrm{P}})^2}} \tag{4.19}$$

the von Mises effective stress with respect to $\boldsymbol{T}_{\text{P}}$. Since $|x|$ is a convex function of x, note that $\langle x \rangle$ is as well. In contrast to the general form (3.13), (4.17) has been assumed explicitly independent of the strain $\boldsymbol{E}$ and inelastic strain $\boldsymbol{E}_{\text{P}}$, in this simple case. More generally, *e.g.*, for the case of deformation-induced anisotropic flow behaviour, this is no longer so (*e.g.*, Svendsen, 2001; Svendsen & Reese, 2003). From (4.17), we have the specific forms

$$\begin{aligned} \dot{\epsilon}_{\text{P}} &= \phi_{,\varsigma_{\text{P}}} = \tfrac{1}{2}\,(1+\text{sgn}(f))\,\sqrt{\tfrac{2}{3}}\,\gamma\,\langle f\rangle^{m} \quad (f \neq 0)\,, \\ \dot{\boldsymbol{E}}_{\text{P}} &= \phi_{,\boldsymbol{T}_{\text{P}}} = \text{sgn}(\text{dev}(\boldsymbol{T}_{\text{P}}))\,\dot{\epsilon}_{\text{P}} \quad (\boldsymbol{T}_{\text{P}} \neq \boldsymbol{0})\,, \end{aligned} \tag{4.20}$$

for $\boldsymbol{E}_{\text{P}}$ and ϵ_{P}, respectively, via the general result (3.12) reduced to the current context. Consequently, $f < 0$ determines the elastic range of the material, and $f > 0$ its inelastic range. In addition,

$$d_{,\dot{\boldsymbol{E}}} = -\phi_{,\dot{\boldsymbol{E}}} = \phi\{(1-\ln f)\,m_{,\dot{\boldsymbol{E}}} - (\ln\gamma)_{,\dot{\boldsymbol{E}}} - (\ln\tau)_{,\dot{\boldsymbol{E}}}\} \quad (f>0) \tag{4.21}$$

follows from (3.13) for the non-equilibrium contribution to $\boldsymbol{S}$ in (4.1). As indicated, ϕ as given by (4.17) is differentiable in ς_{P} everywhere except at $f = 0$, and in $\boldsymbol{T}_{\text{P}}$ everywhere except at $f = 0$ and at $\boldsymbol{T}_{\text{P}} = \boldsymbol{0}$. The corresponding subdifferentials $\dot{\boldsymbol{E}}_{\text{P}} \in \partial_{\boldsymbol{T}_{\text{P}}}\phi$ and $\dot{\epsilon}_{\text{P}} \in \partial_{\varsigma_{\text{P}}}\phi$ exist everywhere.

5 Finite Element Simulation of an Aluminum Tube

Using the standard numerical methods of backward-Euler integration and Newton-Raphson iteration as based on algorithmic or "consistent" linearization (*e.g.*, Simo & Hughes, 1998), the model discussed in the last section can be formulated in algorithmic form and implemented with the help of the finite element method into a numerical simulation of electromagnetic forming. This has been carried out and discussed in detail recently in Brosius *et al.* (2003) for the purpose of simulating the electromagnetic forming of aluminum tubes and of sheet metal at room temperature. As an example of the application of the formulation from the previous section, we discuss here briefly the simulation results for the aluminum tube.

Application of the model from the last section to this case requires in particular the determination of the isotropic hardening behaviour of aluminum. As a first approximation, the quasi-static[2] uniaxial test data of Beerwald *et al.* (2000) for aluminum was used for this purpose. Model identification based on this data yielded the empirical form

$$\psi_{\text{P}}(\epsilon_{\text{P}}) = \sigma_{\text{F}0}\,\epsilon_{\text{P}} + c_1\,(\epsilon_{\text{P}}+c_2)^{c_3} + c_4\,\ln(1+c_5\,\epsilon_{\text{P}}) \tag{5.1}$$

for the dependence $\psi_{\text{P}}(\epsilon_{\text{P}})$ of ψ on ϵ_{P} related to energy storage in the material due to isotropic hardening, with $\sigma_{\text{F}0} = 90$ MPa, $c_1 = 139$ MPa, $c_2 = 0.001$, $c_3 = 0.44$, $c_4 = 12$ MPa, $c_5 = 1609$ and $c_6 = 17$ MPa for Al. The remaining inelastic parameters τ and γ, as well as the strain-rate sensitivity m, have been taken from the literature or estimated. Generally speaking, these are all a function of temperature, strain and strain rate. For the case of conventional forming (*i.e.*, strain rates $|\dot{\boldsymbol{E}}|$ between 0.1 and 10^3 s^{-1}), values for Al of $\tau = 90$ MPa, $\gamma = 6500$ and $m = 4$ have been estimated from the experimental results in Jones (1989). In a similar fashion, we estimated the values $\tau = 90$ MPa, $\gamma = 200000$ and $m = 5$ for the case of electromagnetic forming (*i.e.*, strain rates $|\dot{\boldsymbol{E}}| > 10^3$ s^{-1}). Lastly, at room temperature, aluminum is characterized by the values $\lambda = 39404$ MPa and $\mu = 26269$ MPa for the elastic parameters.

On this basis, a series of finite-element simulations of the electromagnetic forming of an aluminum tube were preformed. The tubes of interest were 40 mm long with a 25 mm outer diamter, 21 mm inner diameter and a wall thickness of 2mm. The finite-element discretization of the tube and symmetry constraints used in the simulation are depicted in Figure 1. Experimentally, the magnetic field is generated parallel to the boundary of the tube. As discussed above in the context of (4.9) and (4.10), in this case the Lorentz force can be represented as a pressure boundary condition. Via the experimentally-determined magnetic field strength (Beerwald *et al.*, 1999, 2000), this pressure boundary condition has been determined for the tube geometry as a function of time and position along the tube axis. Figure 2 depicts this boundary condition as a function of time at the midplane of symmetry shown in Figure 1. Here, the peak magnetic pressure was 63 MPa at 12 μs (Figure 2).

[2]Determination of the hardening behaviour of aluminum during dynamic forming is the subject of work in progress, *e.g.*, Brosius *et al.* (2003).

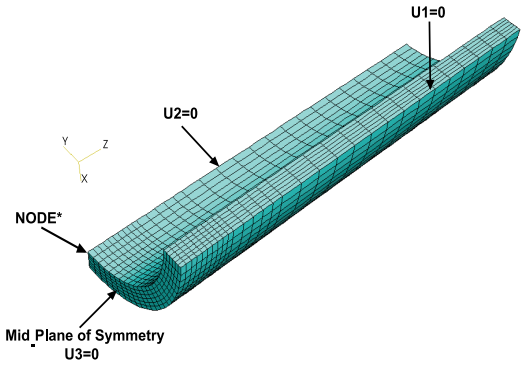

Figure 1. Finite-element mesh and symmetry constraints for the tube simulation.

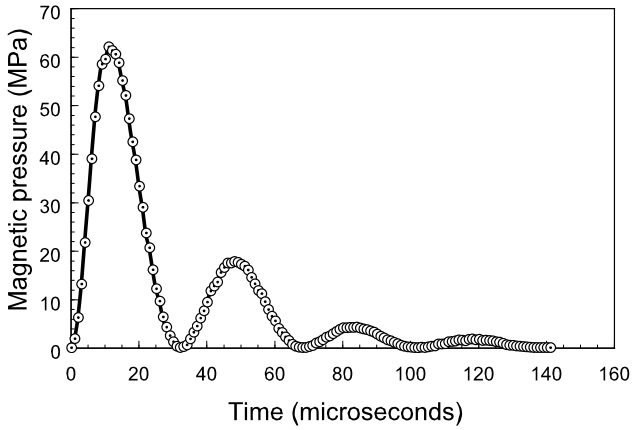

Figure 2. Experimentally-determined dynamic magnetic pressure boundary condition at the midplane of symmetry shown in Figure 1.

Results for a number of such tube simulations are shown in Figures 3 and 4. The results in Figure 3 depict the radial displacement of the tube at the element node indicated in Figure 1 as a function of time and are compared with corresponding experimental results. Here, the simulation results labeled "rate-dependent" were obtained with the elastoviscoplastic model and material parameters discussed in the last section. For comparison, an analogous simulation as based on rate-independent J_2-elastoplasticity and the same isotropic hardening model was carried out. These are the results labeled as "rate-independent" in Figure 3. As expected, at such high strain-rates, and confirmed by these results, inertia has a significant influence on the deformation history of the material. Clearly, neglecting the effect of inertia leads to a substantial overestimation of the effective force acting on the work piece. In addition, the influence of the rate-dependence of the material behaviour on the simulation results is evident. Indeed, because the effective stress driving inelastic deformation is higher than that in the rate-independent J_2 case for corresponding material parameter values, the amount of inelastic and so total deformation achieved in the former case is greater than that in the latter, as confirmed by the results in Figure 3.

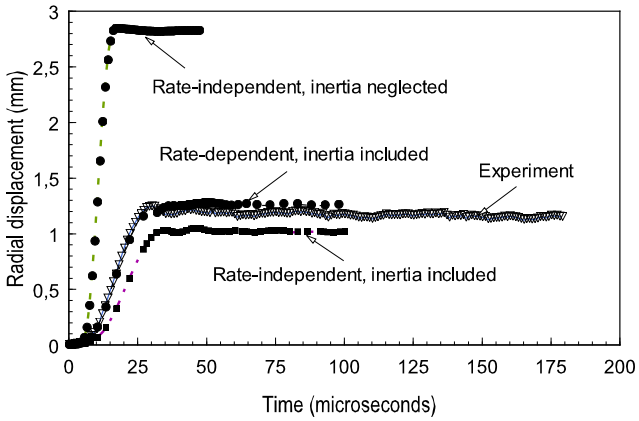

Figure 3. Radial displacement of the tube at node $*$ shown in Figure 1 as a function of time for different simulation conditions compared with experiment. See text for details.

Consider lastly the strain-rate and von Mises stress fields in the tube attained at peak magnetic pressure (Figure 4). As indicated, the maximum strain-rate generated is on the order of 5×10^3 s^{-1} reached in the middle of the tube in its interior. This coincides with the region of maximum driving stress as represented by the von Mises stress as shown in Figure 4. Both of these coincide with the region of maximum attained deformation, *i.e.*, in the middle of the tube. As is the case in Figure 3, the results obtained here as based on rate-dependent modeling agree quantitatively quite well with the rate and amount of forming observed in the experiments.

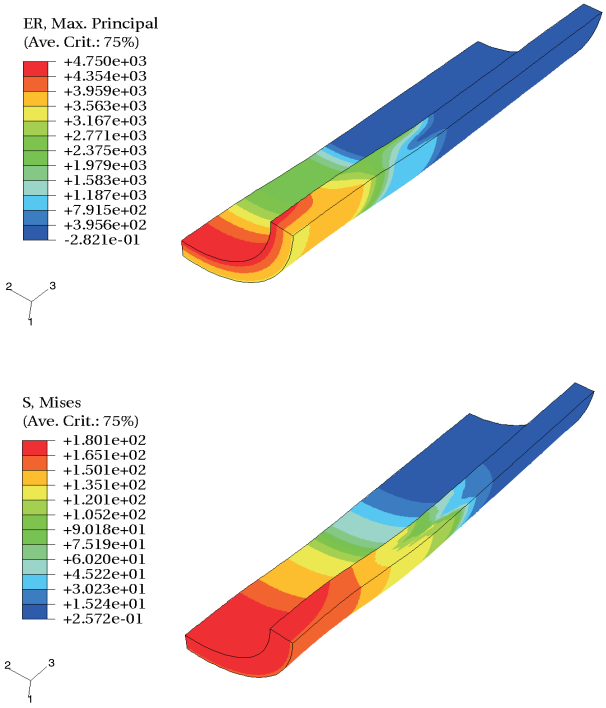

Figure 4. Strain rate and von Mises stress fields in the tube at peak magnetic pressure.

For more details concerning the algorithmic formulation, numerical implementation and further application of the model to other work piece geometries, the reader is referred to Brosius *et al.* (2003).

6 Summary

In this work, we have developed a continuum thermodynamic approach with which one can formulate field and constitutive models in a phenomenological fashion for a class of engineeering materials which can be dynamically formed via strong magnetic fields. The corresponding formulations are based on thermodynamics and internal variables in which the deformation and magnetic fields are in general coupled. This coupling takes the well-known form of the Lorentz force in the momentum balance, as well as that of the electromotive power in the energy balance. In addition, for the case of large deformation, an additional coupling arises due to a dependence of the field relation for the magnetic field on the deformation. Exploitation of the dissipation principle in the current thermodynamic framework yields as usual for the constitutive class of interest thermodynamically consistent material models for generally anisotropic, elastoviscoplastic material behaviour. In particular, the general results so obtained are applied in particular to the case of small strain and large rotation. As shown here, in this special case, the electromagnetic field relations become independent of the deformation field. As such, they can be solved independently and used as input for the solution of the thermomechanical field relations. On the other hand, in the case of large strain, the electromagnetic and thermomechanical field relations are coupled and must be solved simultaneously. Application of the reduced formulation for small strain to the simulation of the electromagnetic forming of an aluminum tube shows the importance of accounting for inertial effects and rate-dependence in the modeling.

Acknowledgements.
The authors wish to thank the reviewers of the first version of this work for helpful comments leading to its improvment. Thanks also go to the Deutsche Forschungsgemeinschaft (DFG) for financial support of the work reported on here under the contract FOR 443/3-1.

References

Beerwald, C.; Brosius, A.; Homberg, W.; Kleiner, M.; Wellendorf, A.: New aspects of electromagnetic forming, in *Proceedings of the 6th International Conference on the Technology of Plasticity*, Volume III, pp. 2471-2476, (1999).

Beerwald, C.; Brosius, A.; Kleiner, M.: Determination of flow stress at very high strain-rates by a combination of magnetic forming and FEM calculation, in *Proceedings of the International Workshop on Friction and Fow Stress in Cutting and Forming* (CIRP), 25.-26.1.2000, ENSAM - Paris, (2000).

Bertram, A.: Description of finite inelastic deformations, in *MECAMAT '92 Multiaxial Plasticity*, Benallal, A., Billardon, R., Marquis, D., editors, pp. 821–835, (1993).

Bruhns, O.; Diehl, H.: An internal variable theory of inelastic behaviour at high rates of strain, *Arch. Mech.* 41, 427–463, (1989).

Brosius, A.; Stiemer, M.; Unger, J.; Blum, H.; Kleiner, M.; Svendsen, B.: Finite-element modeling and simulation of the material and structural behaviour during electromagnetic metal forming of metal tubes and sheet metal, in preparation, (2003).

Edelen, D. G. B.: On the existence of symmetry relations and dissipation potential, *Arch. Rat. Mech. Anal.* 51, 218–227, 1973.

Fenton, G.; Daehn, G. S.: Modeling of electromagnetically formed sheet metal, *J. Mat. Process. Tech.* 75, 6-16, (1998).

Gourdin, W. H.: Analysis and assessment of electromagnetic ring expansion as a high-strain rate test, *J. Appl.* Phys. 65, 411, (1989).

Gourdin, W. H., Weinland, S. L., Boling, R. M.: Development of the electromagnetically-launched expanding ring as a high strain-rate test, *Rev. Sci. Instrum.* 60, 427, (1989).

Hutter, K., van de Ven, A. A. F.: *Field matter interaction in thermoelastic solids*, Lecture Notes in Physics 88, Springer-Verlag, (1978).

Jackson, J. D.: *Classical Electrodynamics*, John Wiley & Sons, (1975).

Jones, N.: *Structural Impact*, Cambridge University Press, (1989).

Lemaitre J.; Chaboche J.-L.: *Mechanics of solid materials*, Cambridge University Press, (1990).

Moon, F.: *Magnetic interactions in solids*, Springer-Verlag, (1980).

Simo, J. C.; Hughes, T. J. R.: *Computational Inelasticity*, Springer Series on Interdisiplinary Applied Mathematics **7**, Springer, (1998).

Šilhavý, M.: *The Mechanics and Thermodynamics of Continuous Media*, Springer-Verlag, (1997).

Svendsen, B.: A thermodynamic formulation of finite-deformation elastoplasticity with hardening based on the concept of material isomorphism. *Int. J. Plasticity* 14, 473–488, (1998).

Svendsen, B.: On the modeling of anisotropic elastic and inelastic material behaviour at large deformation, *Int. J. Solids Structures* 38, 9579–9599, (2001).

Svendsen, B.; Reese, S.: On the modeling of internal variables as structure tensors in anisotropic, finite-deformation inelasticity, *International Journal of Plasticity*, in press, (2003).

Svendsen, B., Chanda, T.: Continuum thermodynamic formulation of models for electromagnetic thermoinelastic solids with application to electromagnetic metal forming, submitted to *Continuumm Mechanics and Thermodynamics*, (2003).

Takata, N., Kato, M., Sato, K., Tobe, T.: High-speed forming of metal sheets by electromagnetic forces, *Japan Soc. Mech. Eng. Int. J.* 31, 142, (1988).

Wang, C. C., Bloom, J.: Material uniformity and inhomogeneity in anelastic bodies, *Arch. Rat. Mech. Anal.* 53, 246–276, (1974).

Address: Professor Dr. Bob Svendsen, Tapas Chanda, Chair of Mechanics, Department of Mechanical Engineering, University of Dortmund, D-44221 Dortmund, Germany.
email: bob.svendsen@udo.edu.